

Supporting Information

**Ferroelasticity, thermochromism, semi-conductivity,
and ferromagnetism in a new layered perovskite:
(4-fluorophenethylammonium)₂[CuCl₄]**

Ya-Ping Gong, Xiao-Xian Chen, Guo-Zhang Huang, Wei-Xiong Zhang* and
Xiao-Ming Chen

MOE Key Laboratory of Bioinorganic and Synthetic Chemistry, School of Chemistry,
Sun Yat-Sen University, Guangzhou 510275, China

Table S1. Crystal data and structure refinement parameters for **1** at RTP, ITP, and HTP.

Compound	1		
Formula	(FPEA) ₂ [CuCl ₄]		
T/K	298(1)	365(1)	415(1)
Phases	RTP	ITP	HTP
Crystal system	monoclinic	monoclinic	orthorhombic
Space group	<i>P2₁/c</i>	<i>A2/m</i>	<i>Cmce</i>
<i>a</i> /Å	20.0414(5)	20.4140(9)	40.211(5)
<i>b</i> /Å	7.3061(2)	7.3636(3)	7.3967(3)
<i>c</i> /Å	7.3103(2)	7.3256(2)	7.3999(4)
$\beta/^\circ$	96.732(2)	100.344(3)	90
<i>V</i> /Å ³	1063.03(5)	1083.29(7)	2201.0(3)
<i>Z</i>	2	2	4
$\rho_{\text{calc}}/\text{g cm}^{-3}$	1.517	1.489	1.466
μ/mm^{-1}	6.251	6.134	6.038
Reflections collected	3816	3423	5878
Independent reflections	2077	1183	1045
$R_1^a/wR_2^b [I \geq 2\sigma(I)]$	0.0449, 0.1234	0.0414, 0.1112	0.0978, 0.2765
R_1^a/wR_2^b (all data)	0.0481, 0.1285	0.0426, 0.1138	0.1262, 0.3325
GOF	1.045	1.120	1.082
CCDC number	2130391	2130394	2130395

^a $R_1 = \sum ||F_o| - |F_c|| / \sum |F_o|$, ^b $wR_2 = \{\sum w[(F_o)^2 - (F_c)^2]^2 / \sum w[(F_o)^2]^2\}^{1/2}$

Table S2. Selected bond lengths (\AA) and bond angles ($^\circ$) for **1** at RTP, ITP, and HTP.

(FPEA) ₂ [CuCl ₄]				
RTP	Cu1–Cl1	2.2866(6)	Cu1–Cl1C	2.8963(6)
	Cu1–Cl1A	2.2866(6)	Cu1–Cl2	2.2978(7)
	Cu1–Cl2A	2.2977(7)	Cl1–Cu1B	2.8963(6)
	\angle Cl1–Cu1–Cl1A	180	\angle Cl1A–Cu1–Cl1B	89.931(5)
	\angle Cl1–Cu1–Cl1B	90.068(5)	\angle Cl1A–Cu1–Cl1C	90.069(5)
	\angle Cl1C–Cu1–Cl1B	180	\angle Cl1–Cu1–Cl1C	89.932(5)
	\angle Cl1–Cu1–Cl2A	90.10(3)	\angle Cl2A–Cu1–Cl1C	88.36(2)
	\angle Cl2A–Cu1–Cl1B	91.64(2)	\angle Cl2–Cu1–Cl1C	91.64(2)
	\angle Cl2–Cu1–Cl1B	88.36(2)	\angle Cl1A–Cu1–Cl2	90.10(3)
	\angle Cl2A–Cu1–Cl2	180		
	A) 1–x, 1–y, –z; B) 1–x, –1/2+y, 1/2–z;; C) +x, 3/2–y, –1/2+z			
ITP	Cu1–Cl2A	2.2870(9)	Cu1–Cl2	2.2870(8)
	Cu1–Cl1B	2.2839(7)	Cu1–Cl1C	2.2839(7)
	Cu1–Cl1D	2.910(2)	Cu1–C1E	2.910(2)
	\angle Cl2A–Cu1–Cl2	180	\angle Cl1D–Cu1–Cl2A	89.83(1)
	\angle Cl1E–Cu1–Cl2	89.83(1)	\angle Cl1–Cu1–Cl2	90.43(17)
	\angle Cl1–Cu1–Cl2A	89.57(17)	\angle Cl1E–Cu1–Cl2A	90.17(1)
	\angle Cl1D–Cu1–Cl2	90.17(1)	\angle Cl1A–Cu1–Cl2A	90.43(17)
	\angle Cl1A–Cu1–Cl2	89.57(17)	\angle Cl1D–Cu1–Cl1	90.25(4)
	\angle Cl1A–Cu1–Cl1	180	\angle Cl1E–Cu1–Cl1A	90.25(4)
	\angle Cl1D–Cu1–Cl1A	89.75(4)	\angle Cl1D–Cu1–Cl1E	180
	\angle Cl1E–Cu1–Cl1	89.75(4)		
	A) 1–x, 1–y, 1–z; B) 1–x, +y, 1–z; C) +x, 1–y, +z; D) 1–x, 1/2+y, 3/2–z; E) 1–x, 1/2–y, –1/2+z.			
HTP	Cu1–Cl2	2.283(4)	Cu1–Cl2A	2.283(4)
	Cu1–Cl1B	2.953(2)	Cu1–Cl1	2.278(2)
	Cu1–Cl1A	2.278(2)	Cl1–Cu1C	2.953(2)
	\angle Cl2A–Cu1–Cl2	180	\angle Cl1A–Cu1–Cl2A	90
	\angle Cl1A–Cu1–Cl2	90	\angle Cl1–Cu1–Cl2A	90
	\angle Cl1–Cu1–Cl2	90	\angle Cl1–Cu1–Cl1A	180
	A) 1–x, 1–y, 1–z; B) +x, –1/2+y, 1/2–z; C) +x, 3/2–y, –1/2+z.			

Table S3. N–H···Cl hydrogen bonds of **1** at RTP, ITP, and HTP.

	D–H···A	<i>d</i> (D–H)	<i>d</i> (H···A)	< DHA	<i>d</i> (D···A)
RTP	N1–H1A···Cl1	0.89	2.39	170.4	3.273(3)
	N1–H1B···Cl2A	0.89	2.50	165.9	3.370(3)
	N1–H1C···Cl1B	0.89	2.65	133.0	3.317(3)
	N1–H1C···Cl2C	0.89	2.80	142.4	3.548(3)
A) $1-x, -1/2+y, 1/2-z$; B) $+x, 3/2-y, 1/2+z$; C) $1-x, 1-y, 1-z$.					
ITP	N1–H1A···Cl1A	0.89	2.64	133.5	3.313(12)
	N1–H1A···Cl1B	0.89	2.76	123.3	3.330(12)
	N1–H1B···Cl1C	0.89	2.51	172.7	3.394(15)
	N1–H1B···Cl2D	0.89	2.53	168.7	3.407(16)
	N1A–H1C···Cl1E	0.89	2.77	129.8	3.414(14)
A) $+x, 1-y, -1+z$; B) $1-x, 1/2+y, 1/2-z$; C) $1-x, 1-y, 1-z$; D) $+x, 1/2+y, -1/2+z$; E) $+x, 1/2-y, -1/2+z$.					
HTP	N1–H1A···Cl1	0.89	2.89	113.96	3.356
	N1–H1A···Cl1A	0.89	2.89	119.01	3.414
	N1–H1B···Cl1B	0.89	2.53	147.28	3.315
	A) $x, y+1/2, -z+1/2$; B) $-x+1, -y+3/2, z+1/2$				

Table S4. The state energies (eV) of the lowest conduction band (L-CB) and the highest valence band (H-VB) of **1**.

<i>k</i>-point	L-CB	H-VB
Z (0.000, 0.000, 0.500)	2.21975	-0.30798
G (0.000, 0.000, 0.000)	2.39111	-0.00032
Y (0.000, 0.500, 0.000)	2.24141	-0.27762
A (-0.500, 0.500, 0.000)	2.24146	-0.27749
B (-0.500, 0.000, 0.000)	2.39114	0
D (-0.500, 0.000, 0.500)	2.21968	-0.30906
E (-0.500, 0.500, 0.500)	2.37831	-0.10966
C (0.000, 0.500, 0.500)	2.37829	-0.10965

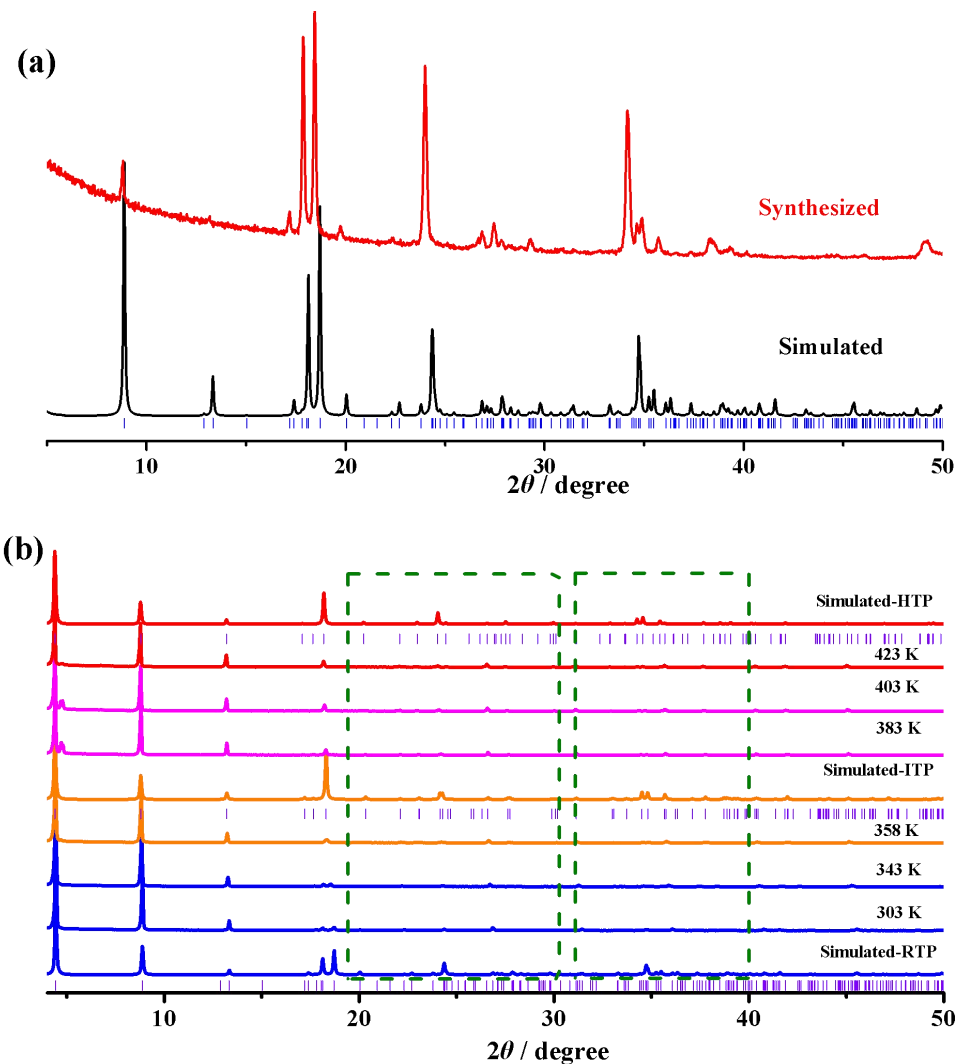


Figure S1. The experimental PXRD pattern of the as-synthesized powder sample (red) and the simulated PXRD pattern (black) based on the single-crystal structure at room-temperature; (b) Variable-temperature PXRD patterns of **1**.

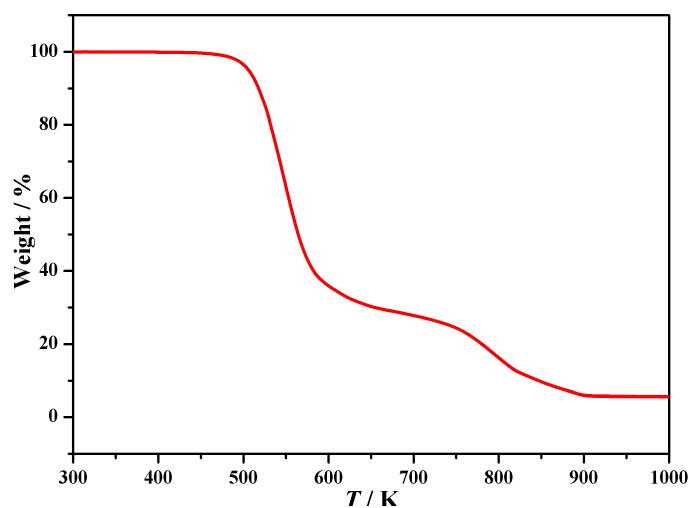


Figure S2. Thermogravimetric analysis (TGA) curve of **1**.

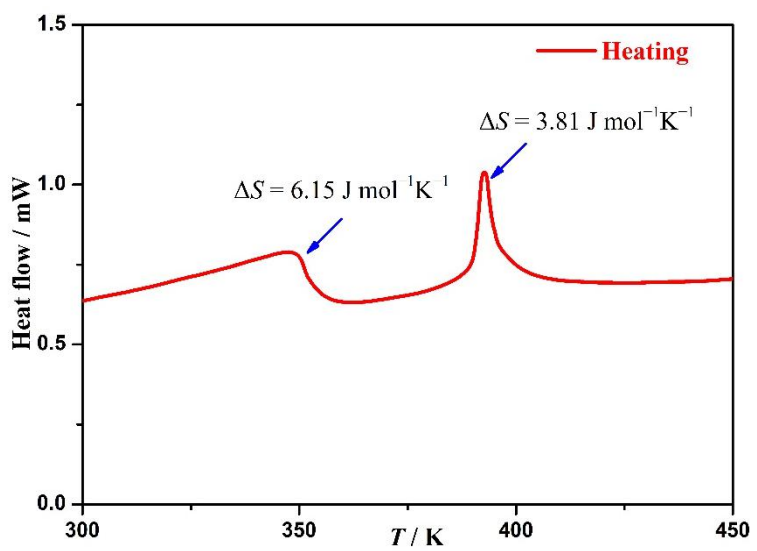


Figure S3. The total entropy changes (ΔS) of phase transitions in the heating process.

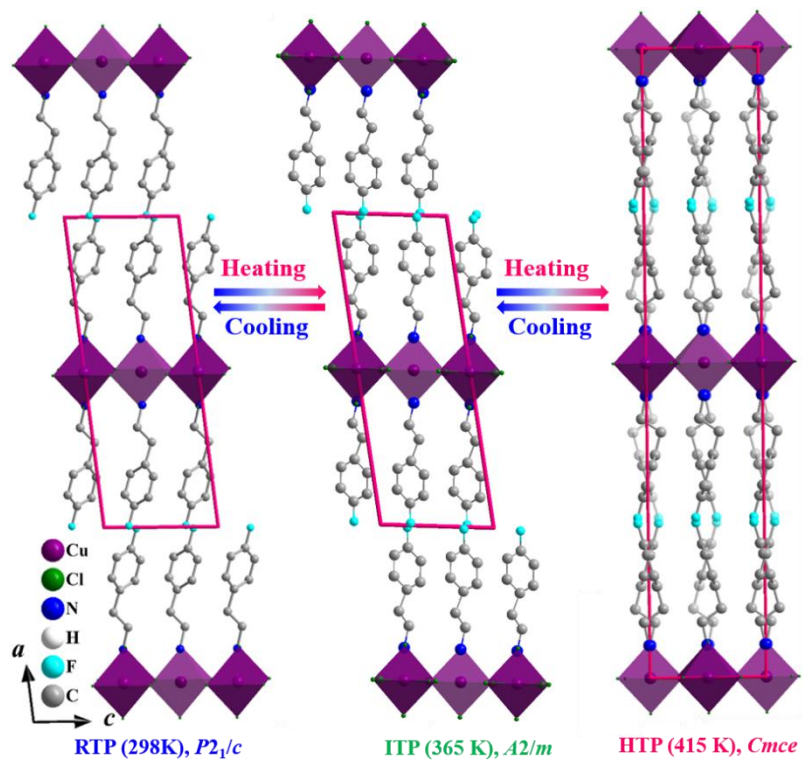


Figure S4. The structures of **1** in RTP, ITP, and HTP viewed along the b axis.

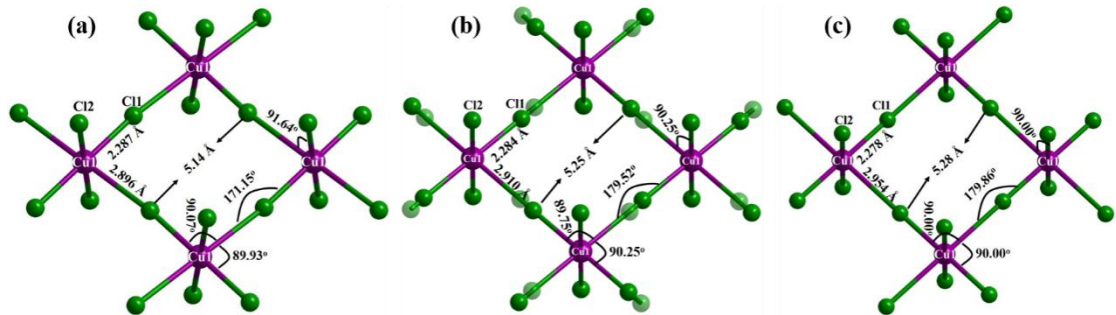


Figure S5. The structural parameters of inorganic layers in RTP, ITP, and HTP.

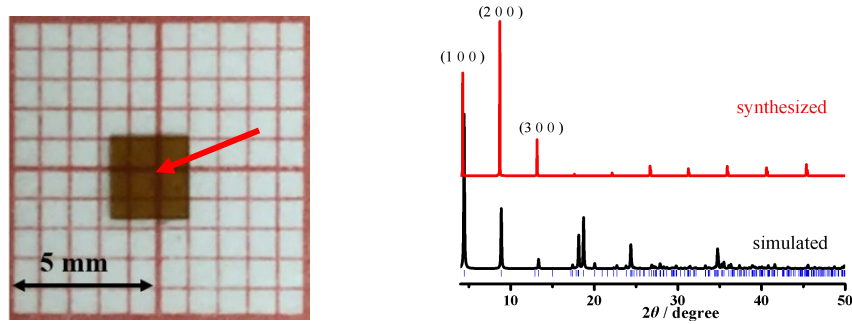


Figure S6. Morphology of a single crystal and its measured PXRD pattern showing that the normal of the largest exposed crystal plane is the a axis.

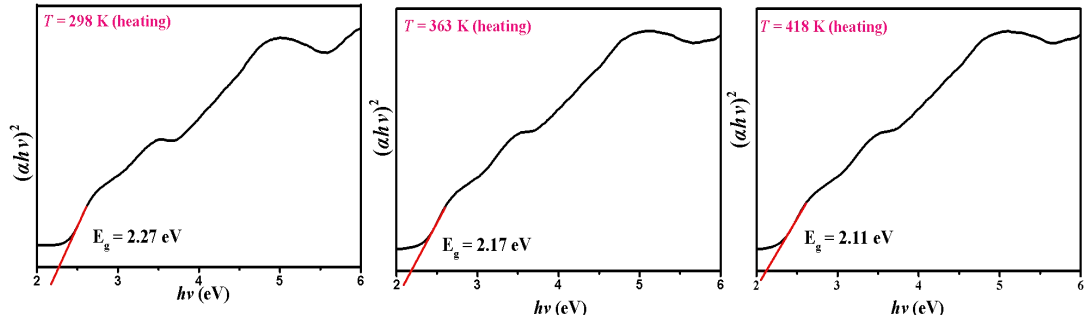


Figure S7. The extrapolated optical band gaps for RTP, ITP, and HTP.

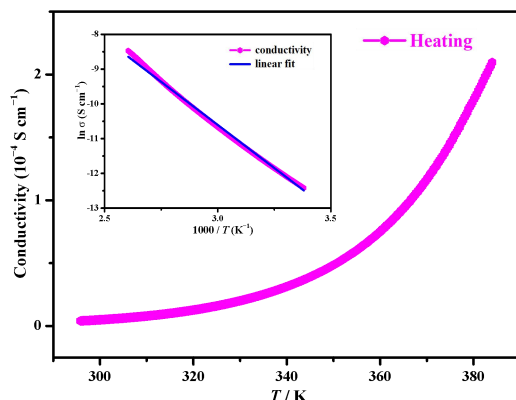


Figure S8. Temperature-dependent conductivity of $(\text{PEA})_2[\text{CuCl}_4]$. Inset: blue line indicates fitting of the data to the Arrhenius equation, yielding an average value for E_a of 0.428 eV.

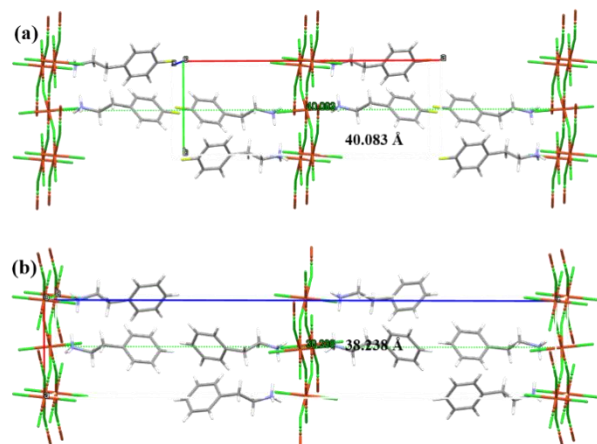


Figure S9. Distance between adjacent inorganic layers of **1** (a) and $(\text{PEA})_2[\text{CuCl}_4]$ (b).

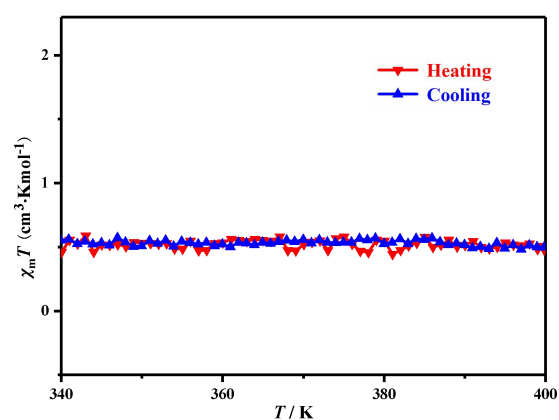


Figure S10. Temperature dependence of $\chi_m T$ measured in a heating-cooling cycle during 340-400 K.

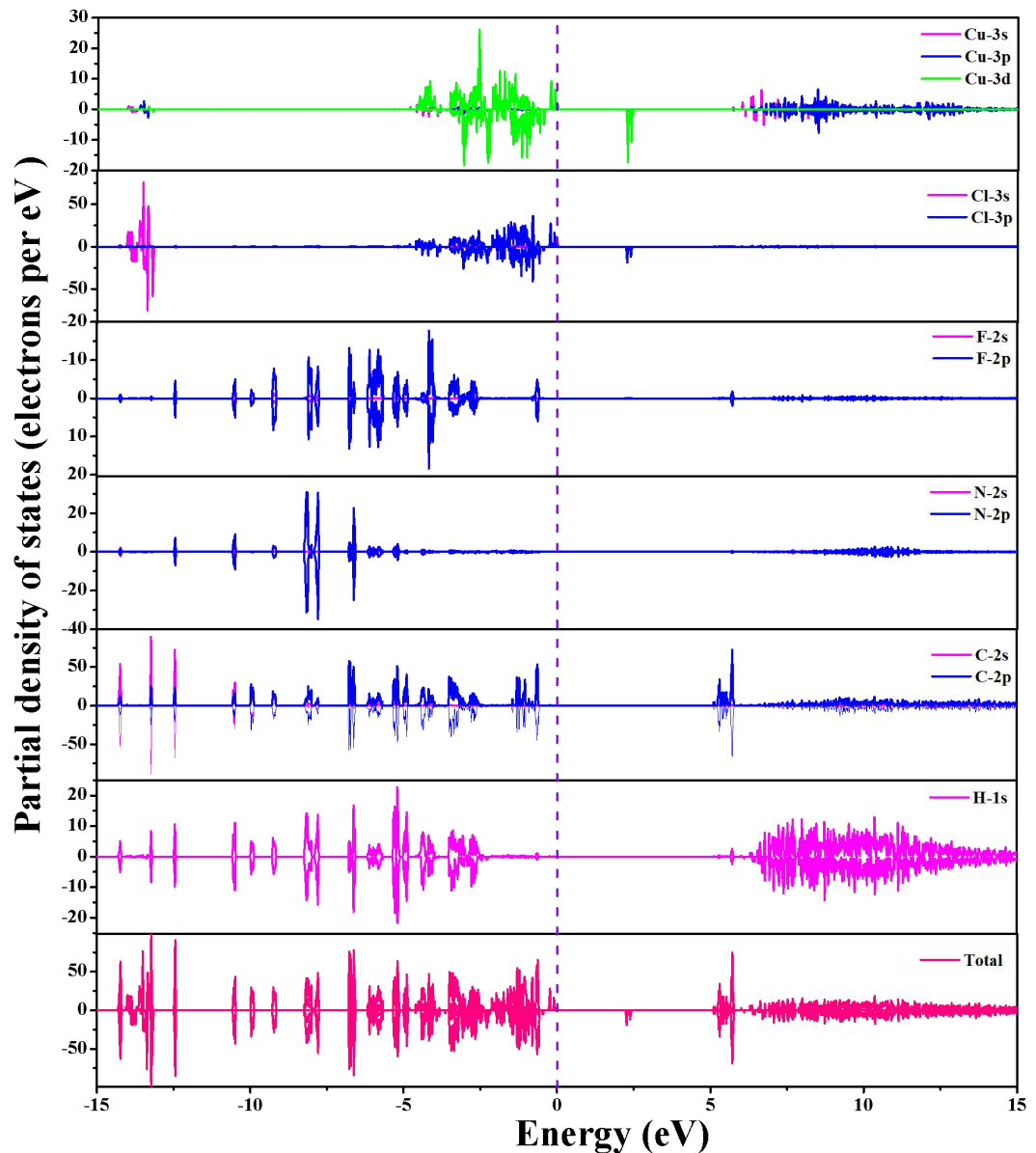


Figure S11. The partial and total density of states of **1**.

Computational Method

The single-crystal structure of $(\text{FPEA})_2[\text{CuCl}_4]$ at 298 K was used for the theoretical calculations. The electron structure calculations and optical properties were performed on the CASTEP code in the Material Studio package,^{S1-S2} a total energy package based on plane-wave pseudopotential method using density functional theory (DFT). The generalized gradient approximation (GGA) of the Perdew-Burke-Ernzerhof for solids (PBEsol) was used for the exchange-correlation energy.^{S3-S4} The following valence-electron configurations were considered in the computation: Cu-3d¹⁰4s¹, Cl-3s²3p⁵, F-2s²2p⁵, C-2s²2p², N-2s²2p³, H-1s¹. The numbers of plane waves included in the basis sets were determined by a cut-off energy of 850 eV. The numerical integration of the Brillouin zone was performed using a Monkhorst-Pack k -point sampling of $1 \times 2 \times 2$.

The calculation of the spontaneous strain

For the present $mmm\text{F}2/m$ species of **1**,^{S5} as the cell setting of orthorhombic lattice is different from the monoclinic one, a necessary conversion matrix, $(0.5 \ 0 \ -0.5 \ 0 \ 1 \ 0 \ 0 \ 0 \ 1)$, was applied for the cell of HTP to match with the monoclinic cell of ITP, giving a converted cell parameters for HTP: $a_0 = 20.443 \text{ \AA}$, $b_0 = 7.397 \text{ \AA}$, $c_0 = 7.400 \text{ \AA}$, $\beta_0 = 100.43^\circ$. Based on geometric relationship, new monoclinic lattice should be:

$$a_0 = \sqrt{\left(\frac{1}{2}a\right)^2 + \left(\frac{1}{2}c\right)^2}$$

$$b_0 = b$$

$$c_0 = c$$

Then the spontaneous strain tensor is given as:⁶

$$\varepsilon_{ij} = \begin{bmatrix} 1 - \frac{a \sin \beta}{a_0 \sin \beta_0} & 0 & \frac{1}{2} \left(\frac{c \cos \beta}{c_0 \sin \beta_0} - \frac{a \cos \beta}{a \sin \beta_0} \right) \\ 0 & 1 - \frac{b}{b_0} & 0 \\ \frac{1}{2} \left(\frac{c \cos \beta}{c_0 \sin \beta_0} - \frac{a \cos \beta}{a \sin \beta_0} \right) & 0 & 1 - \frac{c}{c_0} \end{bmatrix}$$

$$\varepsilon_{ss} = \sqrt{\sum_{ij} \varepsilon_{ij}^2} = 0.011$$

In the equation, a , b , c and β refer to the cell parameters of low-symmetry form ITP, and a_0 , b_0 and c_0 are the converted triclinic cell parameters of high-symmetry form HTP.

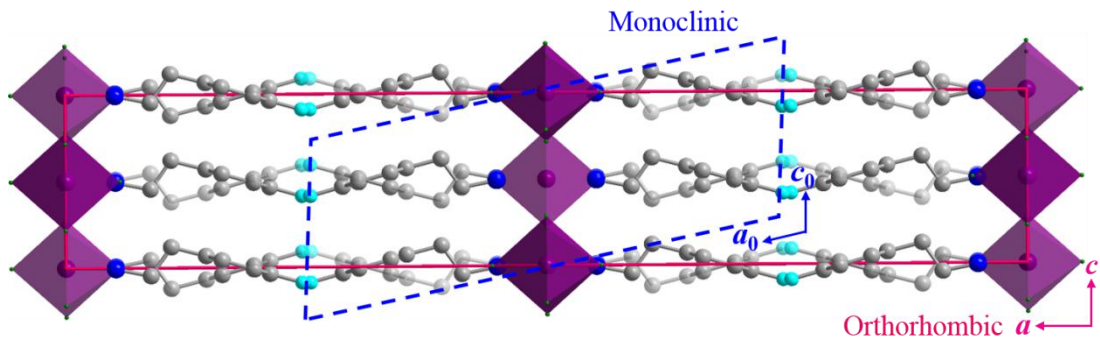


Figure S12. The orthorhombic cell (red) of HTP converted to monoclinic cell (blue) for comparison with the monoclinic unit cell of ITP.

References

- [S1] V. Milman, B. Winkler, J. A. White, C. J. Pickard, M. C. Payne, E. V. Akhmatskaya, R. H. Nobes, *Int. J. Quantum Chem.*, 2000, **77**, 895-910.
- [S2] M. D. Segall, P. J. D. Lindan, M. J. Probert, C. J. Pickard, P. J. Hasnip, S. J. Clark, M. C. J. Payne, *Phys-Condens Mat.*, 2002, **14**, 2717-2744.
- [S3] J. P. Perdew, K. Burke, M. Ernzerhof, *Phys. Rev. Lett.* 1996, **77**, 3865-3868.
- [S4] S. J. Clark, M. D. Segall, C. J. Pickard, P. J. Hasnip, M. J. Probert, K. Refson, M. C. Payne, *Z. Kristallogr.*, 2005, **220**, 567-570.
- [S5] K. Aizu, *J. Phys. Soc. Jpn.*, 1969, **27**, 387-396.
- [S6] K. Aizu, *J. Phys. Soc. Jpn.*, 1970, **28**, 706-716.